Research Article

INTERNATIONAL JOURNAL OF ADVANCED ROBOTIC SYSTEMS

International Journal of Advanced Robotic Systems
March-April 2019: 1–9

DOI: 10.1177/1729881419835626
journals.sagepub.com/home/arx
SAGE

Nonlinear adaptive control with integrated performances for waverider

Liuqing Yang[1,2], Yanbin Liu[3,4] and Yong Zhang[1,2]

Abstract

This article provides a nonlinear controller for waveriders with input saturation to improve transient performances. First, the exact linearization is applied to change an affine nonlinear model to a linear time-invariant model for waveriders. Then, the linear and nonlinear feedback control law is applied for the obtained linearized model for waveriders, and system stability of the presented control law is proved accordingly. Furthermore, the system robustness and improving transient performances are discussed for waveriders. Finally, an example is given for a longitudinal model of the waverider, and the results demonstrate that the closed-loop systems can track the anticipated commands, while guaranteeing the expected integrated performances for waveriders.

Keywords

Waveriders, nonlinear adaptive control, integrated performance, input saturation

Date received: 27 November 2018; accepted: 4 February 2019

Topic: Robot Manipulation and Control
Topic Editor: Andrey V Savkin
Associate Editor: Jose de Jesus Rubio

Introduction

The control design in the nonlinear system for waveriders provides a very challenging work associated with the integrated performance, including input saturation, strong coupling, and considerable uncertainty.[1] The nonlinear inversion is a useful tool in the flight control design depending on converting an affine nonlinear system into a linear time-invariant system for waveriders.[2] Accordingly, some linear time-invariant system control methods are feasible for the nonlinear model of waveriders by combining the state feedback control with the selected linear control law. As such, the nonlinear inversion becomes one of the fruitful methods in the flight control design of waveriders.[3]

There were many research studies done on the nonlinear inversion adopting the feedback linearization method to enhance decoupling control capacity and system robustness for waveriders. In particular, a reference command tracking controller was proposed in the study of Gao and Wang[4] for an air-breathing waverider with parametric uncertainties, and the feedback linearization method based on the H-infinity method was used to address input constraints and to achieve desired tracking performance. Alternatively,

[1] Research Institute of Pilotless Aircraft, Nanjing University of Aeronautics and Astronautics, Nanjing, China
[2] College of Astronautics, Nanjing University of Aeronautics and Astronautics, Nanjing, China
[3] Key Laboratory of Unmanned Aerial Vehicle Technology of Ministry of Industry and Information Technology, Nanjing University of Aeronautics and Astronautics, Nanjing, China
[4] State Key Laboratory of Virtual Reality Technology and Systems, Beihang University, Beijing, China

Corresponding author:
Yanbin Liu, College of Astronautics, Nanjing University of Aeronautics and Astronautics, Nanjing 210016, China.
Email: liuyb@nuaa.edu.cn

a robust control problem was presented in the study of Chen et al.[5] for a control-oriented uncertainty model derived from the feedback linearization approach, and this designed controller was integrated with a high-order sliding mode observer to track the responses of the vehicle to a step change in velocity and altitude with partial state measurements. Unfortunately, it is difficult for the nonlinear inversion-based flight control of waveriders to simultaneously guarantee strong robustness as well as satisfactory transient performance.

On the contrary, there are some novel control strategies presented to improve transient performances of the closed system, such as the improved PD-type iterative learning control technique,[6] robust adaptive control technique,[7–10] composite nonlinear feedback control technique,[11] integral sliding mode control technique,[12–16] and variant-factor technique.[17] However, these control schemes are difficult to directly employ for the nonlinear model of waveriders which have complex flight properties, including strong coupling dynamics, unstable mode, and strong uncertainties. Meanwhile, the input saturation problem in the control design of waveriders should be considered carefully to ensure flight stability. This motivates us to put forward a new tracking controller for waveriders integrating the feedback linearization method and nonlinear control scheme to ameliorate the transient performance. In fact, this adaptive inversion controller can not only guarantee strong robustness and decoupling control ability, but also improve the transient performance for waveriders.

The outline of this article is given as follows. The second section deals with establishing the nonlinear model of waveriders with input saturation. The third section relates to the adaptive control law design for waveriders using the feedback linearization theory and nonlinear output feedback control to make better the transient performance. The fourth section involves the flight performance analysis with special regard to system robustness and tracking response features for waveriders. The fifth section provides an illustrative example of this proposed controller for a nonlinear longitudinal model of the waverider, and the integrated results are compared with those using the dynamic inversion control. Some concluding remarks are provided in the sixth section.

Modeling for waveriders

The model dynamics of the waverider is more complicated in contrast to that of the conventional vehicle, and this is because the structural dynamics affects the aerodynamic properties, whereas the propulsive efficiency is limited by the flight states. In turn, the thrust has a significant impact on the pressure distribution and structural vibration in the forward fuselage, as a result of the strong coupling relations among aerodynamics, propulsion, structure, and control.[18]

Based on the flight dynamics principle, the longitudinal model of a waverider along the speed coordinate system X_V, Y_V, Z_V is identified by[19]

$$\begin{cases} \dot{V} = \frac{T\cos\alpha - D}{m} - g\sin\gamma \\ \dot{\gamma} = \frac{L + T\sin\alpha}{mV} - \frac{g\cos\gamma}{V} \\ \dot{q} = M_y / I_y \\ \dot{\alpha} = q - \dot{\gamma} \\ \dot{h} = V\sin\gamma \end{cases} \tag{1}$$

where V is the flight speed; γ represents the flight path angle; q denotes the change rate with respect to the pitch angle; α indicates the angle of attack; and h is the flight altitude. In addition, m, g, and I_y denote the vehicle mass, gravitational constant, and moment of inertia, respectively. For equation (1), the lift L, drag D, pitch moment M_y, and thrust T determine the flight dynamics of the waverider, and they are calculated by

$$\begin{cases} L = 0.5\rho V^2 s C_L(\alpha, \delta_e) \\ D = 0.5\rho V^2 s C_D(\alpha, \delta_e) \\ M_y = 0.5\rho V^2 s\bar{c} C_M(\alpha, \delta_e) \\ T = T_M \beta \end{cases} \tag{2}$$

where δ_e and β are the elevon deflection angle and propulsive coefficient, respectively; S and $\bar{c}$ indicate the reference area and mean aerodynamic chord, respectively; T_M and ρ represent the maximum thrust and air density, respectively; and C_L, C_D, and C_M denote the respective coefficients with regard to the lift, drag, pitch moment, and thrust. Moreover, the propulsive model is given as a second-order system[20]

$$\ddot{\beta} = -2\xi\varpi\dot{\beta} - \varpi^2\beta + \varpi^2\beta_c \tag{3}$$

where ξ and ϖ denote the damping and frequency of the propulsive system, whereas β_c is the control input regarding the thrust. For simplicity, air density ρ and gravitational constant g are applied as a function of flight height

$$\begin{cases} \rho = f_\rho(h) \\ g = f_g(h) \end{cases} \tag{4}$$

When ignoring the influence of the lift and drag with respect to the elevon deflection in the control design, the corresponding aerodynamic coefficients are expressed by[21]

$$\begin{cases} C_L = f_L(\alpha) \\ C_D = f_D(\alpha) \\ C_M = f_{M_y}(\alpha, q) + f_{\delta_e}\delta_e \end{cases} \tag{5}$$

where f_{δ_e} represents the moment coefficient with respect to the elevon. Furthermore, for equations (1) to (5), the nonlinear model of the waverider is reshaped as

$$\begin{cases} \dot{X} = f(X) + G(X)U \\ y = H(X) \end{cases} \tag{6}$$

where the flight state vector X is selected as $X = [V, \gamma, \alpha, \beta, h]'$; the control input vector U is defined as $U = [\delta_e, \beta_c]'$; and the output vector is given as $y = [V, h]'$. In addition, $G = [g_\delta, g_\beta]'$ indicates the input matrix; whereas f, H, g_δ, and g_β represent, respectively, the vectors determined by the longitudinal airplane model in equations (1) to (4). Therefore, this nonlinear model of the waverider can be considered as a two-input-two-output nonlinear system.

For the nonlinear model of the waverider, we first use the feedback linearization method to build an equivalent model. Considering the nonlinear model in equation (6), we assume that f, H, g_δ, and g_β are smooth. Correspondingly, the Lie derivative of the function H along f is adopted by[22]

$$L_f H = \frac{\partial H}{\partial X} f(X) \tag{7}$$

The equivalent model corresponding to the nonlinear model (equations (1) to (4)) is gotten by[23]

$$\begin{cases} \dot{z}_1 = z_2 \\ \dot{z}_2 = z_3 \\ \dot{z}_3 = L_f^3 V + \left(L_{g_\beta} L_f^2 V\right)\beta_c + \left(L_{g_\delta} L_f^2 V\right)\delta_e \end{cases} \tag{8}$$

$$\begin{cases} \dot{z}_4 = z_5 \\ \dot{z}_5 = z_6 \\ \dot{z}_6 = z_7 \\ \dot{z}_7 = L_f^4 h + \left(L_{g_\beta} L_f^3 h\right)\beta_c + \left(L_{g_\delta} L_f^3 h\right)\delta_e \end{cases} \tag{9}$$

where $X_V = [z_1, z_2, z_3]' = [V, L_f V, L_f^2 V]'$ and $X_h = [z_4, z_5, z_6, z_7]' = [h, L_f h, L_f^2 h, L_f^3 h]'$. For simplicity, this equivalent model can also be reshaped as[24]

$$\begin{bmatrix} V^{(3)} \\ h^{(4)} \end{bmatrix} = \begin{bmatrix} V_0^{(3)} \\ h_0^{(4)} \end{bmatrix} + \begin{bmatrix} p_{11} & p_{12} \\ p_{21} & p_{22} \end{bmatrix} \begin{bmatrix} \delta_e \\ \beta_c \end{bmatrix} = s + pU \tag{10}$$

According to equation (10), we find that the resulting model has full vector relative degree $r = 7$, which is equal to the order number of the nonlinear model (equations (1) to (4)). Such result indicates that the nonlinear model can be completely linearized if equation (5) is satisfied.[25]

Nonlinear control for waveriders

After the above transformation, let $\Upsilon_V = V^{(3)}$ and $\Upsilon_h = h^{(4)}$, the obtained equivalent model in equation (10) is rewritten as follows

$$\begin{cases} \dot{X}_V = A_V X_V + B_V \Upsilon_V, Y_V = V = C_V X_V \\ \dot{X}_h = A_h X_h + B_h \Upsilon_h, Y_h = h = C_h X_h \end{cases} \tag{11}$$

$$A_V = \begin{bmatrix} 0 & 1 & 0 \\ 0 & 0 & 1 \\ 0 & 0 & 0 \end{bmatrix}, \quad B_V = \begin{bmatrix} 0 \\ 0 \\ 1 \end{bmatrix}, \quad C_V[1 \quad 0 \quad 0]$$
$$A_h = \begin{bmatrix} 0 & 1 & 0 & 0 \\ 0 & 0 & 0 & 1 \\ 0 & 0 & 0 & 1 \\ 0 & 0 & 0 & 0 \end{bmatrix}, \quad B_h \begin{bmatrix} 0 \\ 0 \\ 0 \\ 1 \end{bmatrix}, \quad C_h = [1 \quad 0 \quad 0 \quad 0] \tag{12}$$

Furthermore, we consider the input saturation regarding the vehicle model, so the control design goal is to develop a nonlinear control law so that the outputs $y = [V, h]'$ can asymptotically follow the references $y_c = [V_c, h_c]'$. To this end, the equivalent model in equations (11) and (12) is yielded as

$$\begin{cases} \dot{z} = Az + Bv, v = s(z) + p(z)\text{sat}(U) \\ y = Cz \end{cases} \tag{13}$$

where $z = [X_V, X_h]' = [z_1, z_2, z_3, z_4, z_5, z_6, z_7]' = \Phi(X)$, $U = [u_V, u_h]' = [\beta_c, \delta_e]'$, whereas sat shows the saturation function, and the resulting system matrices are expressed as $A = \text{diag}(A_V, A_h)$, $B = \text{diag}(B_V, B_h)$, and $C = \text{diag}(C_V, C_h)$.

Beyond this, we define a reference generator for the equivalent model[26]

$$\begin{cases} \dot{\bar{z}} = A\bar{z} + Bv_e, \\ v_e = F_e\bar{z} + r_s \\ r = C\bar{z} \end{cases} \tag{14}$$

where $\bar{z} \in \Re^7$ is the state of the reference generator; F_e indicates the feedback gain matrix; and r_s represents the virtual signal source. This reference generator can provide an arbitrary type of output signal, including the sinusoidal signal and ramp signal by choosing F_e and r_s. In addition, defining $z_e = z - \bar{z}$, and then based on equations (13) and (14), we obtain

$$\begin{cases} \dot{z}_e = Az_e + B(v - v_e), \\ v = s(z) + p(z)\text{sat}(U) \\ v_e = F_e\bar{z} + r_s \\ \tilde{z} = y - r = C(z - \bar{z}) = Cz_e \end{cases} \tag{15}$$

This error equation is used in the design of the nonlinear control law. Furthermore, a nominal point $x_n \in X$ is selected so that $z_n = \Phi(x_n)$ and $z_n \in Z$. Then, for a set of scalars $\tau_i \in (0, 1), i = V, h$, let $\mu > 0$ be the largest positive scalar such that for all $x \in X_{iV}$, where[27]

$$X_{iV} := \{x : x'Px \le \mu\} \tag{16}$$

the following condition holds

$$||e_i' p^{-1}(z_n)||||B'Px|| \le (1-\tau_i)\bar{u}_i, \quad i = V, h \tag{17}$$

where $e_i \in \Re^2$ is a vector in which only the ith element of e_i is 1 and the others are zero. Following that, we provide the following theorem.

Theorem 1. Suppose that

1. $f(x)$ and $g_i(x), i = V, h$ are smooth vector fields and $H(x)$ is a smooth function on a compact and connected set X of $\Re^7$.
2. The relative degree of the nonlinear model is $(r_V, r_h)'$ on X.
3. $p(z) = (p_V(z), p_h(z))$ is invertible at $z \in Z$ in which $z = \Phi(x)$ is non-singular on X.

Then, the nonlinear control law is designed as

$$u : \begin{pmatrix} u_V \\ u_h \end{pmatrix} = p^{-1}(z)[Fz_e + v_e + \rho(z_e)B'Pz_e - s(z)] \tag{18}$$

where

$$(A+BF)'P + P(A+BF) = -W \tag{19}$$

for $P > 0$ and $W \in \Re^{7\times 7}$ represents a positive definite symmetric matrix, whereas F is chosen such that (1) $A + BF$ is an asymptotically stable matrix and (2) the closed-loop system $C(sI - A - BF)^{-1}B$ has the expected properties. In addition, $p(z)$ should be different to zero to avoid singularities in the controller, and $\rho(z_e)$ indicates the nonpositive vector function regarding z_e.

Thus, the control law comprising equations (18) and (19) will drive system output y to track arbitrary reference r from an initial state asymptotically without steady-state error, provided that the following properties are satisfied.

1. There exist a set of scalars, $\tau_i \in (0,1), i = V, h$ so that

$$||e_i' p^{-1}(z)Fz_e - e_i' p^{-1}(z)s(z)|| \le \tau_i \bar{u}_i, i = V, h \tag{20}$$

2. $\rho(z_e) = \mathrm{diag}(\rho_V, \rho_h)$ and ρ_i is a continuous function for $i = V, h$. Let $x_n \in X$ be a given nominal value so that

$$p_i < 0, \quad \text{and} \quad \sigma_{\min}(R_p) > 0, \quad \forall z \in Z \tag{21}$$

where $R_p := p(z, z_0)p^{-1}(z_n, z_{0,n})$, $z_n = \Phi(x_n)$, and $z_n \in Z$. $\sigma_{\min}$ denotes the minimal singular value.

3. Let x_{iV} be the initial value of x. Then, the initial condition z_{eV} of z_e satisfies

$$z_{eV} \in X_{iV}, \quad z_{eV} = \Phi(X_{iV}) \tag{22}$$

Proof. Consider $z_e = z - \bar{z}$, then

$$\begin{aligned} u &= p^{-1}(z)[Fz_e + v_e + \rho B'Pz_e - s(z)] \\ &= p^{-1}(z)\rho B'Pz_e + p^{-1}(z)[Fz_e + v_e - s(z)] \end{aligned} \tag{23}$$

When $z_e \in X_{iV}$, it shows that

$$||e_i' p^{-1}(z_n)||||B'Pz_e|| \le (1-\tau_i)\bar{u}_i, \quad i = V, h \tag{24}$$

Note that $\sigma_{\min}\left(R_p(z)\right) \neq 0$ on Z due to the assumption that $p(z)$ is invertible on the compact and connected Z. Furthermore, when $0 \le ||\rho|| \le \sigma_{\min}(R_p)$, we have

$$\begin{aligned} ||e_i' p^{-1}(z)\rho|| &\le ||e_i' p^{-1}(z)||||\rho|| \\ &\le ||e_i' p^{-1}(z)||\sigma_{\min}(R_p) \\ &\le ||e_i' p^{-1}(z)R_p|| = ||e_i' p^{-1}(z_n)|| \end{aligned} \tag{25}$$

for $i = V, h$. Thus, according to equations (24) and (25)

$$\begin{aligned} ||e_i' p^{-1}(z)\rho(\tilde{z})B'Pz_e|| &\le ||e_i' p^{-1}(z)\rho(\tilde{z})||||B'Pz_e|| \\ &\le ||e_i' p^{-1}(z_n)||||B'Pz_e|| \le (1-\tau_i)\bar{u}_i \end{aligned} \tag{26}$$

for $i = V, h$. Afterward, with equations (23) and (26)

$$\begin{aligned} ||u_i|| &= ||\, e_i' p^{-1}(z)\rho(\tilde{z})B'Pz_e + e_i' p^{-1}(z)[Fz_e + v_e - s(z)]\,|| \\ &\le ||e_i' p^{-1}(z)\rho B'Pz_e|| + ||e_i' p^{-1}(z)[Fz_e + v_e - s(z)]|| \\ &\le (1-\tau_i)\bar{u}_i + \tau_i \bar{u}_i = \bar{u}_i \end{aligned} \tag{27}$$

for $i = V, h$. Thus

$$\begin{aligned} \mathrm{sat}(u) &= [sat(u_V), sat(u_h)]' \\ &= p^{-1}(z)[Fz_e + v_e + \rho B'Pz_e - s(z)] \end{aligned} \tag{28}$$

When $0 < \sigma_{\min}(R_p) \le ||\rho||$

$$\begin{aligned} u_i &= e_i' p^{-1}(z)\rho B'Pz_e + e_i' p^{-1}(z)[Fz_e + v_e - s(z)] \\ &= e_i' p^{-1}(z)\tilde{\rho}B'Pz_e + e_i' p^{-1}(z)[\rho_\sigma B'Pz_e + Fz_e + v_e - s(z)] \end{aligned} \tag{29}$$

for $i = V, h$, $\tilde{\rho} = \rho_\sigma - \rho$, and $\rho_\sigma = -\sigma_{\min}(R_p) - \varepsilon$ where ρ_i is substituted into $-\sigma_{\min}(R_p)$ if $|\rho_i| > \sigma_{\min}(R_p)$ for $i = V, h$ and ε is a given small positive number such that $\tilde{\rho}$ is invertible.

For the results as $0 < \sigma_{\min}(R_p) \le ||\rho||$, the second item in equation (29) can be limited as follows

$$|e_i' p^{-1}(z)[\rho_\sigma B'Pz_e + Fz_e + v_e - s(z)]| \le \bar{u}_i \tag{30}$$

for $i = V, h$. Thus

$$\begin{aligned} [\mathrm{sat}(u_V), \mathrm{sat}(u_h)]' &= qp^{-1}(z)\tilde{\rho}B'Pz_e \\ &\quad + p^{-1}(z)[\rho_\sigma B'Pz_e + Fz_e + v_e - s(z)] \end{aligned} \tag{31}$$

where $q = \mathrm{diag}(q_V, q_h)$ and $q_i \in [0,1]$ for $i = V, h$. Finally

$$\begin{aligned} [\mathrm{sat}(u_V), \mathrm{sat}(u_h)]' &= p^{-1}(z)[p(z)qp^{-1}(z)\tilde{\rho}B'Pz_e \\ &\quad + \rho_\sigma B'Pz_e + Fz_e + v_e - s(z)] \end{aligned} \tag{32}$$

Based on equations (28) and (32), we obtain the following result

$$[\mathrm{sat}(u_V), \mathrm{sat}(u_h)]' = p^{-1}(z)[\bar{\rho}B'Pz_e + Fz_e + v_e - s(z)] \tag{33}$$

where

$$\bar{\rho} = \begin{cases} \rho \\ p(z)qp^{-1}(z)\tilde{\rho} + \rho_\sigma \end{cases} \tag{34}$$

Moreover, substituting equations (33) and (34) into equation (15), we have

$$\dot{z}_e = Az_e + B(\bar{\rho}B'Pz_e + Fz_e) = (A + B\bar{\rho}B'P + BF)z_e \tag{35}$$

We choose a Lyapunov function below

$$\Gamma = z_e'Pz_e \tag{36}$$

Then, the derivative of Γ can be computed with equations (19) and (34) as follows

$$\begin{aligned} \dot{\Gamma} &= z_e'(-W + PB\bar{\rho}'B'P + PB\bar{\rho}B'P)z_e \\ &= -z_e'Wz_e + z_e'PB\left[\tilde{\rho}(p^{-1})'qp' + pqp^{-1}\tilde{\rho} + 2\rho_\sigma\right]B'Pz_e \\ &= -z_e'Wz_e + z_e'PB(2\rho_\sigma)B'Pz_e - z_e'PB\left[(-\tilde{\rho})(p')^{-1}qp' + pqp^{-1}(-\tilde{\rho})\right]B'Pz_e \\ &= -z_e'Wz_e + z_e'PB(2\rho_\sigma)B'Pz_e - z_e'PBR_\rho\left(p'_\rho{}^{-1}qp'_\rho + p_\rho qp_\rho^{-1}\right)R_\rho B'Pz_e \\ &\le -z_e'Wz_e < 0 \end{aligned} \tag{37}$$

where $R_\rho = (-\tilde{\rho})^{1/2}$, $p_\rho = p_\rho{}^{-1}p(z)$, and $\lambda_{\min}(p'_\rho{}^{-1}qp'_\rho + p_\rho qp_\rho^{-1}) = 2_{\min}(q_v, q_h) \ge 0$. These results indicate that once $z_{eV} \in X_{iV}$, z_{eV} will never be out of X_{iV} as $\dot{\Gamma} < 0$ if equations (20) and (21) are satisfied. In other words, the initial value of z_{eV} is met with $z_{eV} \in X_{iV}$, z_{eV} will lie in X_{iV} on the basis of $\dot{\Gamma} < 0$. Thus, the closed-loop system including equations (15) and (18) is asymptotically stable. This accomplishes the proof of this theorem.

Performance analysis for adaptive inversion control

From the evaluating viewpoint of the control demands, first the consumed energy for the tracking response is required to be taken into account for the waverider. According to the total energy principle, if the aerodynamic drag force is neglected, the expected minimum energy in the control process is expressed by[28]

$$E_{\min} = 0.5m(V_c - V_0)^2 + mg(h_c - h_0) \tag{38}$$

In fact, the control energy is far more than that in equation (38) due to the presence of the aerodynamic drag and uncertain disturbance. Accordingly, the energy change rate is given as

$$\dot{E}_T = m\dot{V}V + mg\dot{h} = \mathrm{m}V(\dot{V} + g\sin\gamma + \dot{E}_D) \tag{39}$$

where $\dot{E}_D$ represents the energy consumption rate due to overcoming the drag. By integrating equation (39), the needed control energy is obtained by

$$E_T = \int_{t=0}^{t_s} \dot{E}_T \mathrm{d}t \tag{40}$$

where t_s denotes flight duration time. Based on equations (39) and (40), the control performances among the distinct control laws can be compared from the viewpoint of the consumed energy. Such performance index is very important for the waverider because the carried fuel is strictly limited. Besides the direct energy calculation, the control performances are also compared for the different control laws in terms of the quadratic cost function

$$J_T = \int_{t=0}^{t_s} (X^T Q_X X + U^T Q_U U)\mathrm{d}t \tag{41}$$

where Q_X and Q_U are the according weighting factors. From equation (41), we know such performance index reflects the coordinating relations between the flight states and control inputs, further determining the control energy feature. In addition, the overshoot percentages of the altitude and velocity can be calculated by

$$\begin{cases} \sigma_V = \frac{V_{\max} - V_c}{V_c - V_0} \times 100\% \\ \sigma_h = \frac{h_{\max} - h_c}{h_c - h_0} \times 100\% \end{cases} \tag{42}$$

where $V_{\max}$ and $h_{\max}$ indicate the maximum values with regard to the altitude and velocity in tracking process. Beyond these, setting time t_{Vs} and t_{hs} corresponding to the altitude and velocity commands are defined as the shortest time durations when the response curves keep within 5% of the commands.

In general, the nonlinear adaptive control can improve dynamic performance, enhance system robustness, and implement tracking response. Thus, the following section will provide an illustrative example to test the advantages of the proposed controller for the waverider.

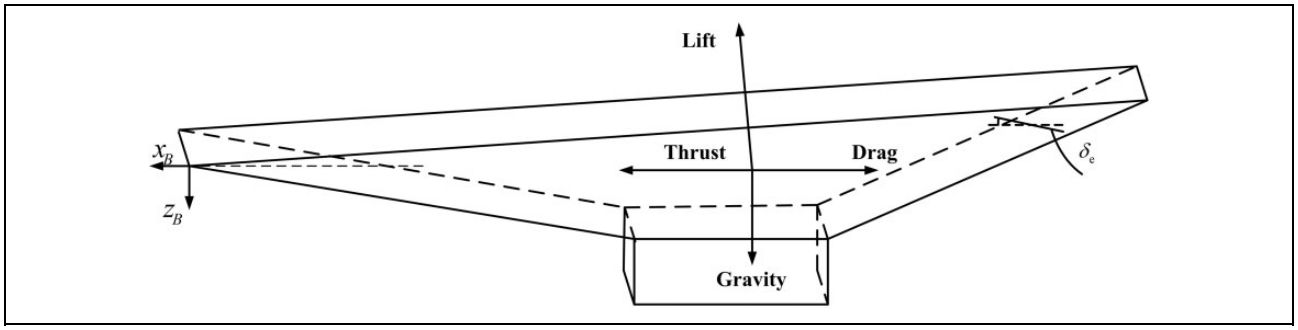

Figure 1. Free body diagram of waveriders.

Illustrative example

This article uses the waverider model proposed by Bolender and Doma[29] to validate the feasibility of the presented control law, and a free body diagram is provided in Figure 1. Correspondingly, the flight control law is employed for the nonlinear model of the waverider to show the improved transient performance in comparison to that with the control law designed with the traditional control method.

By using the least-squares fitting methods for these aerodynamic coefficients obtained from the work of Bu and Wang,[30] the resulting aerodynamic expressions with regard to $V_0 = 2392.5\text{m/s}$, $h_0 = 26\text{km}$ are approximately acquired. Beyond this, we select the linear feedback law gains

$$\begin{cases} F_V = [1 \quad 2 \quad 5] \\ F_h = [0.5 \quad 2 \quad 5 \quad 5] \end{cases} \tag{43}$$

Next, we choose W_V and W_h as the identity matrices, respectively. Afterward, the nonlinear gain functions in equation (18), which can decrease the chattering and improve the transient performance, are selected as

$$\begin{cases} \rho_V = -3|e^{-0.1|e_V|}| \\ \rho_h = -0.4|e^{-0.05|e_h|}| \end{cases} \tag{44}$$

In the simulation, passing through 100 s the response curves are acquired corresponding to $h_c = h_0 + \Delta h_c = 26.1\text{km}$, $V_c = V_0 + \Delta V_c = 2472.5\text{m/s}$. They are shown in Figures 2 and 3.

Figure 2 demonstrates that the velocity and altitude outputs can follow the command signals rapidly. Also, Figure 3 shows the change curves of the angle of attack and control inputs gently return to the anticipated balance values depending on the control action. Moreover, the error change curves regarding the consumed energy and quadratic cost index in equations (40) and (41) are provided in Figure 4.

Figure 4 demonstrates that the control energy using the proposed control law is less than that using the traditional control law, and simultaneously the performance index of this controller is better than that using the traditional

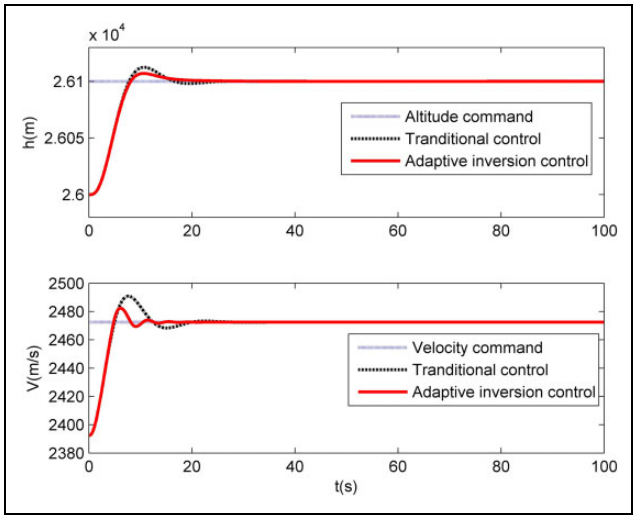

Figure 2. Contrast curves between adaptive inversion control and traditional control.

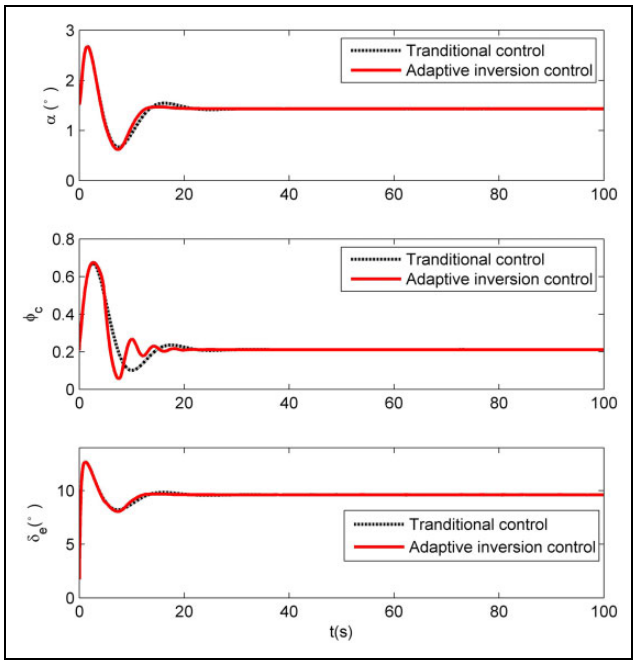

Figure 3. Angle of attack and control inputs between adaptive inversion control and traditional control.

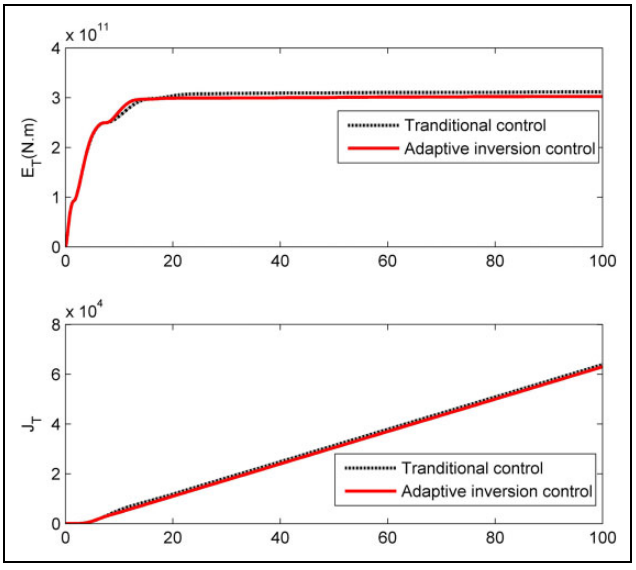

Figure 4. Control consumed energy and quadratic cost index.

Table 1. Dynamic performance indices in the track process.

	Our control	Traditional control
σ_V (%)	7.03	12.48
σ_h (%)	12.36	22.95
t_{Vs} (s)	7.51	15.46
t_{hs} (s)	13	14.17

control law. Such results display the adaptive inversion control can guarantee the optimal control consequence in comparison to the control law designed based on the traditional control law. Furthermore, the dynamic performance indices with regard to the overshoot and setting time in equation (42) are given in Table 1.

According to Table 1, we know that the dynamic performance indices using the flight control law with the adaptive inversion control are better than those using the traditional control law. For example, setting time decreases dramatically due to the existence of the nonlinear part. Besides that, we further take into account the model uncertainties, given by

$$\begin{cases} \bar{L} = L(1 \pm 20\% \Delta I_L) \\ \bar{D} = D(1 \pm 20\% \Delta I_D) \\ \bar{M}_y = M_y(1 \pm 30\% \Delta I_M) \end{cases} \tag{45}$$

where ΔI_L, ΔI_D, and ΔI_M denote the random disturbances between 0 and 1. Once these uncertain items are exerted, the model features will change accordingly. Not only these uncertainties in equation (45), but also the influence of the elevator lift will be introduced such that the airplane model becomes a non-minimum phase system. Once the control law is applied based on Theorem 1, the corresponding results are shown in Figures 5 and 6.

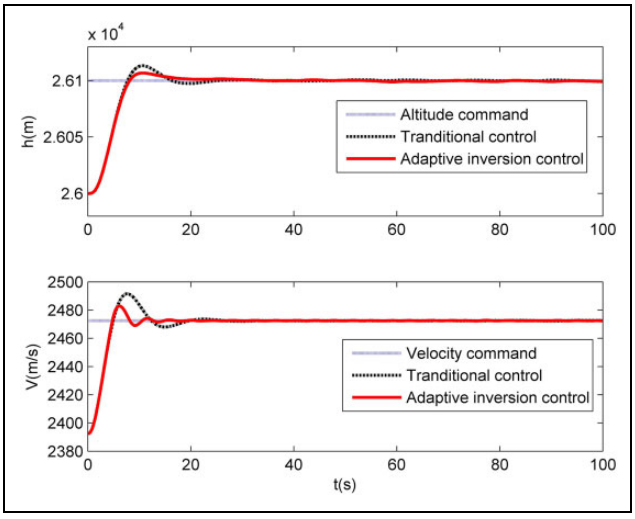

Figure 5. Track response curves for uncertain model.

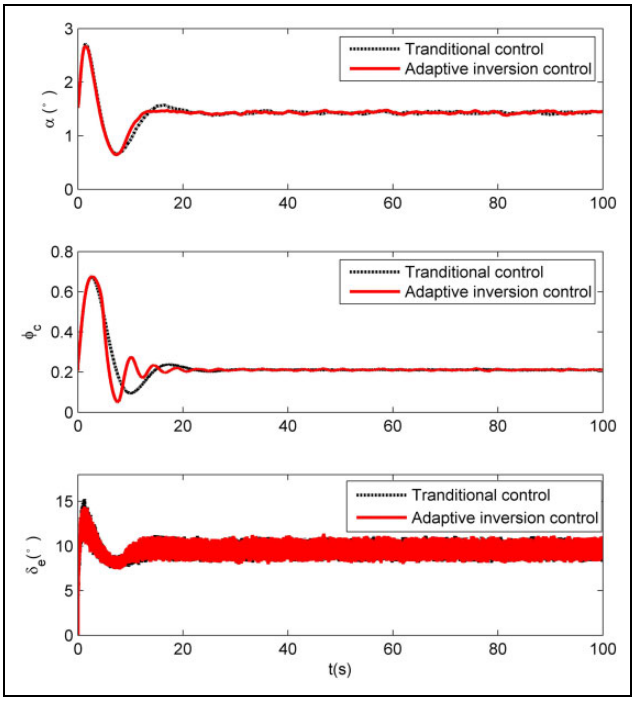

Figure 6. Angle of attack and control inputs for uncertain model.

From Figures 5 and 6, we observe that the response results are satisfactory even in case of the large uncertainties, and the velocity and altitude tracking errors keep small as the response process enters to the steady state. In addition, the angle of attack and control inputs appear to jigger due to the uncertain effects, surrounding with the respected steady values. Alternatively, the undesired chattering in Figure 6, which is induced by the model uncertainties and sat function, will be ameliorated using the nonlinear gain functions, and this indicates that the control action can not only maintain system stability, but also guarantee strong robustness.

Conclusion

This article proposes a nonlinear adaptive control law for the waverider, and the results indicate that the proposed control law improves the transient performance. More importantly, strong robustness of the closed-loop system is guaranteed for the waverider even while considering the large uncertain disturbances as well as the input saturation. Nevertheless, it should be noted that, in this article, we have assumed that all flight states can be measured to feedback, thus the future work is to research the state observers for this presented control law such that these flight states can be estimated as a result of satisfying the requirements in the real application.

Declaration of conflicting interests

The author(s) declared no potential conflicts of interest with respect to the research, authorship, and/or publication of this article.

Funding

The author(s) disclosed receipt of the following financial support for the research, authorship, and/or publication of this article: This work is supported by Fundamental Research Funds for the Central Universities under Grant numbers NZ2018008 and NS2017060, and the open funding project of State Key Laboratory of Virtual Reality Technology and Systems under Grant number VRLAB2018C04.

ORCID iD

Liuqing Yang https://orcid.org/0000-0003-1990-9321

References

1. Fiorentini L, Serrani A, Bolender MA, et al. Nonlinear robust adaptive control of flexible air-breathing hypersonic vehicles. *J Guid Control Dyn* 2009; 32(2): 401–416.
2. Johnson EN, Calise AJ, Curry MD, et al. Adaptive guidance and control for autonomous hypersonic vehicles. *J Guid Control Dyn* 2006; 29(3): 725–737.
3. Wang Q and Stengel RF. Robust nonlinear control of a hypersonic aircraft. *J Guid Control Dyn* 2000; 23(4): 577–585.
4. Gao G and Wang JZ. Reference command tracking control for an air-breathing hypersonic vehicle with parametric uncertainties. *J Franklin Inst Eng Appl Math* 2013; 350(5): 1155–1188.
5. Chen B, Liu Y, Lei H, et al. Ascent trajectory tracking for an air-breathing hypersonic vehicle with guardian maps. *Int J Adv Robot Syst* 2017; 14(3): 1–11.
6. Chen FM, Tsai JSH, Liao YT, et al. An improvement on the transient response of tracking for the sampled-data system based on an improved PD-type iterative learning control. *J Franklin Inst Eng Appl Math* 2014; 351(2): 1130–1150.
7. de Jesus Rubio J. Robust feedback linearization for nonlinear processes control. *ISA Transact* 2018; 74(2): 155–164.
8. Wang HQ, Liu XP, Li S, et al. Adaptive neural output-feedback control for a class of nonlower triangular nonlinear systems with unmodeled dynamics. *IEEE Trans Neural Netw* 2018; 29(8): 3658–3668.
9. de Jesus Rubio J, Pieper J, Meda-Campaña JA, et al. Modelling and regulation of two mechanical systems. *IET Sci Measure Technol* 2018; 12(5): 657–665.
10. Sun YG, Qiang HY, Mei X, et al. Modified repetitive learning control with unidirectional control input for uncertain nonlinear systems. *Neural Comput Appl* 2018; 30(6): 2003–2012.
11. Chen BM, Lee TH, Peng K, et al. Composite nonlinear feedback control for linear systems with input saturation: theory and an application. *IEEE Trans Automat Control* 2003; 48(3): 427–439.
12. Chen Z, Cong BL, and Liu XD. A robust attitude control strategy with guaranteed transient performance via modified Lyapunov-based control and integral sliding mode control. *Nonlinear Dyn* 2014; 78(3): 2205–2218.
13. de Jesus Rubio J, Soriano E, Felipe JC, et al. Sliding mode regulator for the perturbations attenuation in two tank plants. *IEEE Access* 2017; 5(8): 20504–20511.
14. Kumar J, Kumar V, and Rana KP. Design of robust fractional order fuzzy sliding mode PID controller for two link robotic manipulator system. *J Intelligent Fuzzy Syst* 2018; 35(5): 5301–5315.
15. de Jesus Rubio J. Hybrid controller with observer for the estimation and rejection of disturbances. *ISA Transact* 2016; 65(3): 445–455.
16. Alrifai MT and Zribi M. Sliding mode control of chaos in a single machine connected to an infinite bus power system. *Mathl Prob Eng* 2018; 12(2): 1–12.
17. Peng K and Chen BM. Variant factor technique for tracking control of a class of nonlinear systems with input saturation. *Control Intelligent Syst* 2013; 41(3): 169–177.
18. Wilcox ZD, MacKunis W, Lind BL, et al. Lyapunov-based exponential tracking control of a hypersonic aircraft with aerothermoelastic effects. *J Guid Control Dyn* 2010; 33(4): 1213–1224.
19. Liu YB, Deng J, and Lu YP. Preliminary research on optimal design based on control demands for hypersonic morphing vehicle. *IEEE Aerospace Electronic Syst Magazine* 2013; 28(5): 23–31.
20. Hu XX, Wu LG, Hu CH, et al. Adaptive sliding mode tracking control for a flexible air-breathing hypersonic vehicle. *J Franklin Inst Eng Appl Math* 2012; 349(2): 559–577.
21. Parker JT, Serrani A, Yurkovich S, et al. Control-oriented modeling of an air-breathing hypersonic vehicle. *J Guid Control Dyn* 2007; 30(3): 856–869.
22. Marrison CI and Stengel RF. Design of robust control systems for a hypersonic aircraft. *J Guid Control Dyn* 1998; 21(1): 58–63.
23. Rehman OU, Petersen IR, and Fidan B. Feedback linearization-based robust nonlinear control design for

hypersonic flight vehicles. *Proc Inst Mech Eng Part I J Syst Contr Eng* 2013; 227(11): 3–11.
24. Sun HB, Li SH, and Sun CY. Finite time integral sliding mode control of hypersonic vehicles. *Nonlinear Dyn* 2013; 73(1): 229–244.
25. Yang F, Yuan RY, and Yi JQ. Direct adaptive type-2 fuzzy neural network control for a generic hypersonic flight vehicle. *Soft Comput* 2013; 17(11): 2053–2064.
26. Cheng G, Peng K, Chen BM, et al. Improving transient performance in tracking general references using composite nonlinear feedback control and its application to high-speed *XY*-table positioning mechanism. *IEEE Trans Indus Electron* 2007; 54(2): 1039–1051.
27. Lan W, Chen BM, and He Y. On improvement of transient performance in tracking control for a class of nonlinear systems with input saturation. *Syst Control Letters* 2006; 55(2): 132–138.
28. Schmidt DK and Hermann JA. Use of energy-state analysis on a generic air-breathing hypersonic vehicle. *J Guid Control Dyn* 1998; 21(1): 71–76.
29. Bolender MA and Doma DB. Nonlinear longitudinal dynamical model of an air-breathing hypersonic vehicle. *J Spacecraft Rockets* 2007; 44(2): 374–387.
30. Bu X and Wang Q. Neural network-based nonaffine control of air-breathing hypersonic vehicles with prescribed performance. *Int J Adv Robot Syst* 2008; 15(2): 1–15.